ACADEMIC PRESS

Available online at www.sciencedirect.com
SCIENCE DIRECT®

NeuroImage

NeuroImage 19 (2003) 42–63

www.elsevier.com/locate/ynimg

Detection of cortical transition regions utilizing statistical analyses of excess masses

Oliver Schmitt,[a,*] Lars Hömke,[b] and Lutz Dümbgen[c]

[a] *Institute of Anatomy, University of Rostock, Gertrudenstr. 9, D-18055 Rostock, Germany*
[b] *Institute of Mathematics, Medical University of Lübeck, Wallstrasse 40, D-23560 Lübeck, Germany*
[c] *Department of Mathematical Statistics and Actuarial Science, University of Berne, Sidlerstrasse 5, CH-3012 Berne, Switzerland*

Received 3 May 2002; revised 15 November 2002; accepted 26 November 2002

Abstract

A new statistical approach for observer-assisted detection of transition regions of adjacent cytoarchitectonic areas within the human cerebral cortex was developed. This method analyzes the structural information of cytoarchitectural profiles (e.g., the modality of a gray level intensity distribution) based on observed excess mass differences verified by a suitable statistical test. Profiles were generated by scanning the cerebral cortex over respective regions of interest that were oriented to trajectories running parallel to the orientation of cell columns. For each single profile, determination of excess masses provided evidence for a certain number of peaks in the cell density, thereby avoiding fluctuation due solely to sampling anomalies. Comparing such excess mass measurements by means of multiple local rank tests over a wide range of profiles allowed for the detection of cytoarchitectural inhomogeneities at respective given confidence levels. Special parameters (e.g., level of significance, width of targeted region, number of peaks) then could be adapted to specific pattern recognition problems in lamination analyses. Such analyses of excess masses provided a general tool for observer-assisted evaluation of profile arrays. This observer-assisted statistical method was applied to five different cortical examples. It detected the same transition regions that had been determined earlier through direct examination of samples, despite cortical convexities, concavities, and some minor staining inhomogeneities.

Keywords: Brain mapping; Neuroimaging; Cerebral cortex; Cytoarchitecture; Lamination; Excess mass; Multiple local rank test; Transition regions; Profiles; Traverses; Trajectories

Introduction

The subdivision of the human cerebral cortex into distinct regions or areas is based on various previously described microstructural modalities, such as descriptive cytoarchitectonics (Campbell, 1905; Smith, 1907; Brodmann, 1909; von Economo and Koskinas, 1925; Bailey and von Bonin, 1951; Sarkissov et al., 1955), myeloarchitectonics (Vogt and Vogt, 1919), pigmentarchitectonics (Braak, 1980), and angioarchitectonics (Pfeifer, 1940; Duvernoy, 1979). The specific loss of neuronal functionality due to physical damage was identified through lesion mapping (Kleist, 1934). Today, in vivo functional mapping by PET, MRI, and EEG procedures provides far more accurate information to help us understand the relationships between structure and function at different spatiotemporal resolutions (Orrison et al., 1985; Frackowiak et al., 1997). Our understanding of cytoarchitectonic parcellation of the cerebral cortex has been expanded further by additional studies of microstructural modalities using such analytical techniques as receptorautoradiography (receptorarchitectonics) (Zilles et al., 1991, 1996; Geyer et al., 1997, 1998), chemoarchitectonics (Nieuwenhuys, 1985; Preuße and Schmitt, 1998, 1999b,a), quantitative cytoarchitectonics (Schleicher et al., 1999, 2000), and extracellular matrix visualization (Hilbig et al., 2001). Quantitative analysis of the cytoarchitecture of the cerebral cortex is applied to localize changes or inhomogeneities in the laminar and columnar patterns of

* Corresponding author.
E-mail address: schmitt@med.uni-rostock.de (O. Schmitt).

1053-8119/03/$ – see front matter © 2003 Elsevier Science (USA). All rights reserved.
doi:10.1016/S1053-8119(03)00040-5

cell arrangements. Structural changes in cell arrangements or regional cytoarchitecture are indicators of a transition from one cytoarchitectonic field to another, assuming that such a transition involves no changes to the pattern of layering or microstructure (Roland and Zilles, 1998). These cytoarchitectonic transitions may subdivide a cortical area into subareas, or they may indicate a border to another area. Such structural inhomogeneities frequently indicate functionally distinct regions (examples: the transition from Brodmann area 6 to area 4 or from area 4 to area 3a). Transition regions may be detected by quantitative analysis (Schleicher et al., 2000) or through qualitative and/or descriptive methods (Campbell, 1905; Smith, 1907; Brodmann, 1909; Bailey and von Bonin, 1951; Sarkissov et al., 1955). The latter methods may result in overparcellation or underparcellation of microstructurally defined cortical areas, leading to confusion and nonacceptance of the architectonic subdivision (Lashley and Clark, 1946; Clark, 1952). Thus, it is necessary to perform subdivisions of the cerebral cortex using methods that can generate reproducible results.

Despite the fact that there are many different microstructural modalities, microfunctional correlations to specific cell arrangements were found by (Luppino et al., 1991). However, later studies have not shown that spatial distribution patterns of neurons (e.g., cluster spherical, cluster laminations, hard core processes, Poisson processes) are necessary conditions for specific neurophysiological processes (Schmitt et al., 2000). An investigation of the individual neuronal morphology provides evidence for the "morphology influences physiology" hypothesis (Krichmar and Nasuto, 2002). Further structural features, such as connectivity, synapse distribution, receptor expression, and substances involved in neuronal information transfer, are necessary for function-associated neuronal processing. Therefore, cytoarchitectonic changes are nonspecific indicators for certain microfunctional changes (Roland and Zilles, 1998), but specific indicators for the delineation of cortical areas. Areas that appear to be homogenous with regard to their distribution of constitutive structural elements may subsequently reveal structural inhomogeneities when these areas are subjected to concise spatial analysis.

Typically, in order to find structural changes, test lines (traverses) must be generated orthogonal to the neuronal lamination or perpendicular to the cortical surface. The pixel intensities along one traverse can be plotted as a profile diagram (Hudspeth et al., 1976; Schleicher and Zilles, 1990; Schleicher et al., 1999, 2000). Such a profile represents the lamination at a certain point of the cerebral cortex. Scanning the cortical path by consecutive traverses generates a series of profiles or a profile array called a cortical fingerprint (Hudspeth et al., 1976). Through a new method reported herein, the traverses are generated by a new robust approach based on an electrodynamic model developed by Schmitt and Böhme (2002). By applying transformations in order to reduce low-pass noise such as staining inhomogeneities, background staining, variations in staining intensity of cell bodies, or illumination artifacts of the digitized images when calculating the gray level index (GLI) image (Schleicher et al., 1978, 1986, 1987), a viable starting point for performing cortex analysis is reached. In GLI images, traverses can be generated in the same way as in original nontransformed images. The pixels (gray values or GLI values) which are hit by a traverse are selected and written into a vector called a profile.

Transitions between two distinct cytoarchitectonic areas may be detected by comparing profiles of the cortical fingerprint (Hudspeth et al., 1976). Yet it is advantageous if such a detection algorithm also involves a statistical test to determine if a transition of the profile data is significant. Schleicher et al. (1987, 1998, 1999) developed a technique based on Hotellings T^2 test (Bartels, 1979, 1981) for the Mahalanobis (Mahalanobis et al., 1949) distance measure of feature vectors. Feature vectors comprise central mean, moments, central moments, first derivatives of those, and z-value normalizations (Schleicher et al., 1998, 1999). As a result of this approach salient transition from area 17 to area 18 and the blurred transition from area 18 to area 19 have been shown to be statistically significant. Furthermore, Geyer et al. (1996) proved by means of this technique that the predicted subparcellation of area 4 (Zilles et al., 1995) into a rostral area 4a and a posterior area 4p is significant. This method leads to statistically verifiable results and can be employed for detecting transition regions which were previously unknown.

A weakness of the latter methods is that statistical moments (Amunts et al., 2000) do not provide suitable quantities to allow an accurate description of the number and strength of peaks in a profile. That means the intrinsic structural information of the profiles is not taken into account, although this information would seem to be most important for the detection of structural changes in the

Fig. 1. (a) Digitized whole section through both occipital lobes. The left and right hemispheres are represented as equidistant. (b) The ROI of the section through the right hemisphere is enlarged and the inner and outer contours which are defined as interactive are shown. (c) The arrows point to the start and stop positions of traverse generation. A single traverse is marked at the bottom and the areas 17 (A17 red), 18 (A18 blue), and 19 (A19 green) are delineated. (d) The profile of the start traverse is presented in this diagram. (e) All profiles are collected in a profile array where the transition regions are marked in red (T18-19, T19-18, T18-17) and the areas are written in black in between arrows. The pial surfaces within the profile arrays are always at the top and the white matter border is always at the bottom. (f) The profile arrays are analyzed by EMA and significant increases in interval combinations are summarized in the UP diagram, whereas significant decreases in interval combinations are indicated in the DOWN diagram. The same transition regions as in (c) and indicated in (e) are surrounded by red boxes. Artifacts (microfoldings and tears) which produce significant jumps are highlighted by two green boxes indicating the disturbed location in the profile array. Such wrong positive significant inhomogeneities must be critically compared with the original image and profile array data.

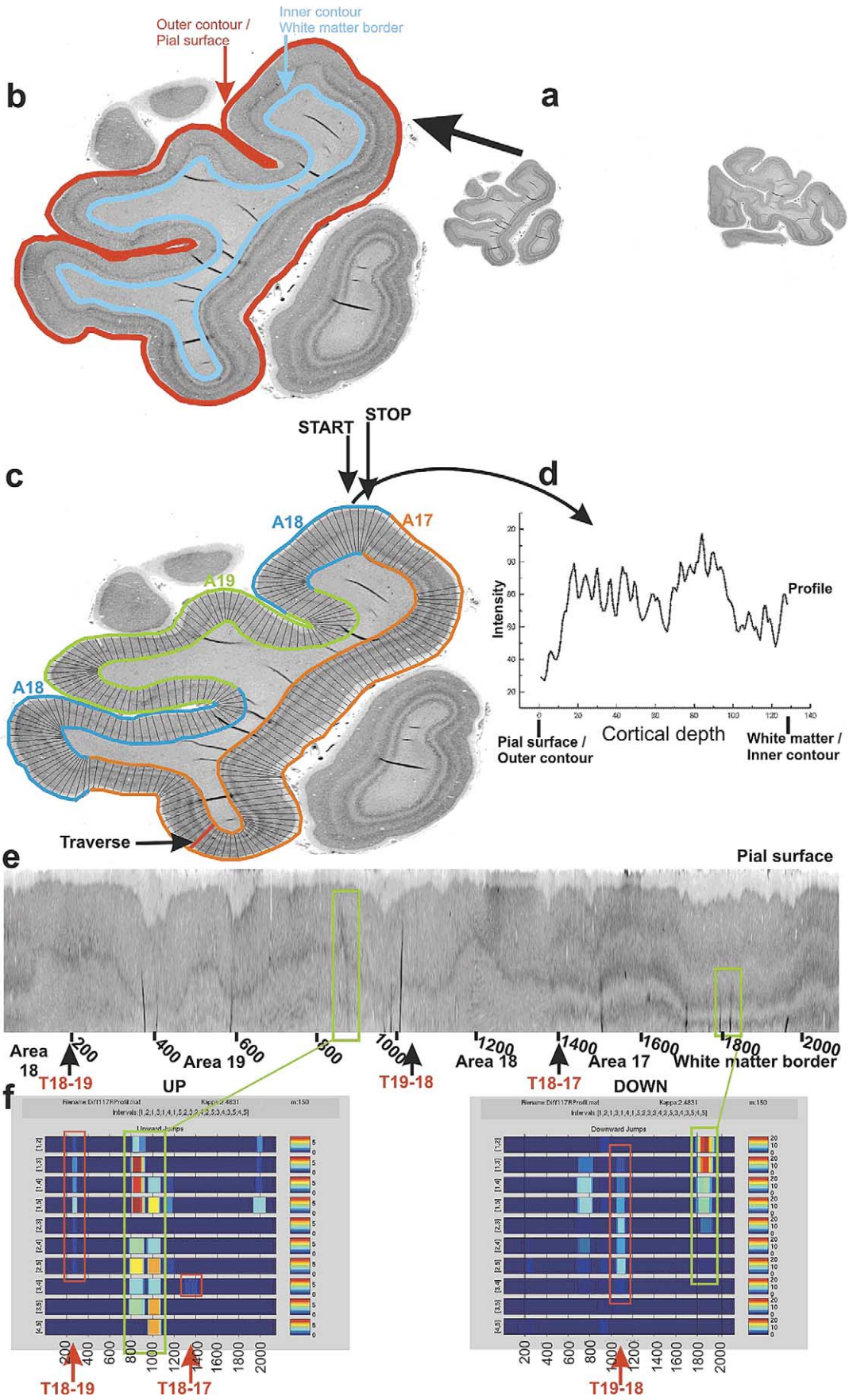
Outer contour / Pial surface
Inner contour White matter border
b
a
START
STOP
c
d
A18
A17
A19
A18
Traverse
Intensity
Profile
Pial surface / Outer contour
Cortical depth
White matter / Inner contour
e
Pial surface
Area 18
Area 19
Area 18
Area 17
White matter border
T18-19
UP
T19-18
T18-17
DOWN
f
Downward Jumps
T18-19
T18-17
T19-18

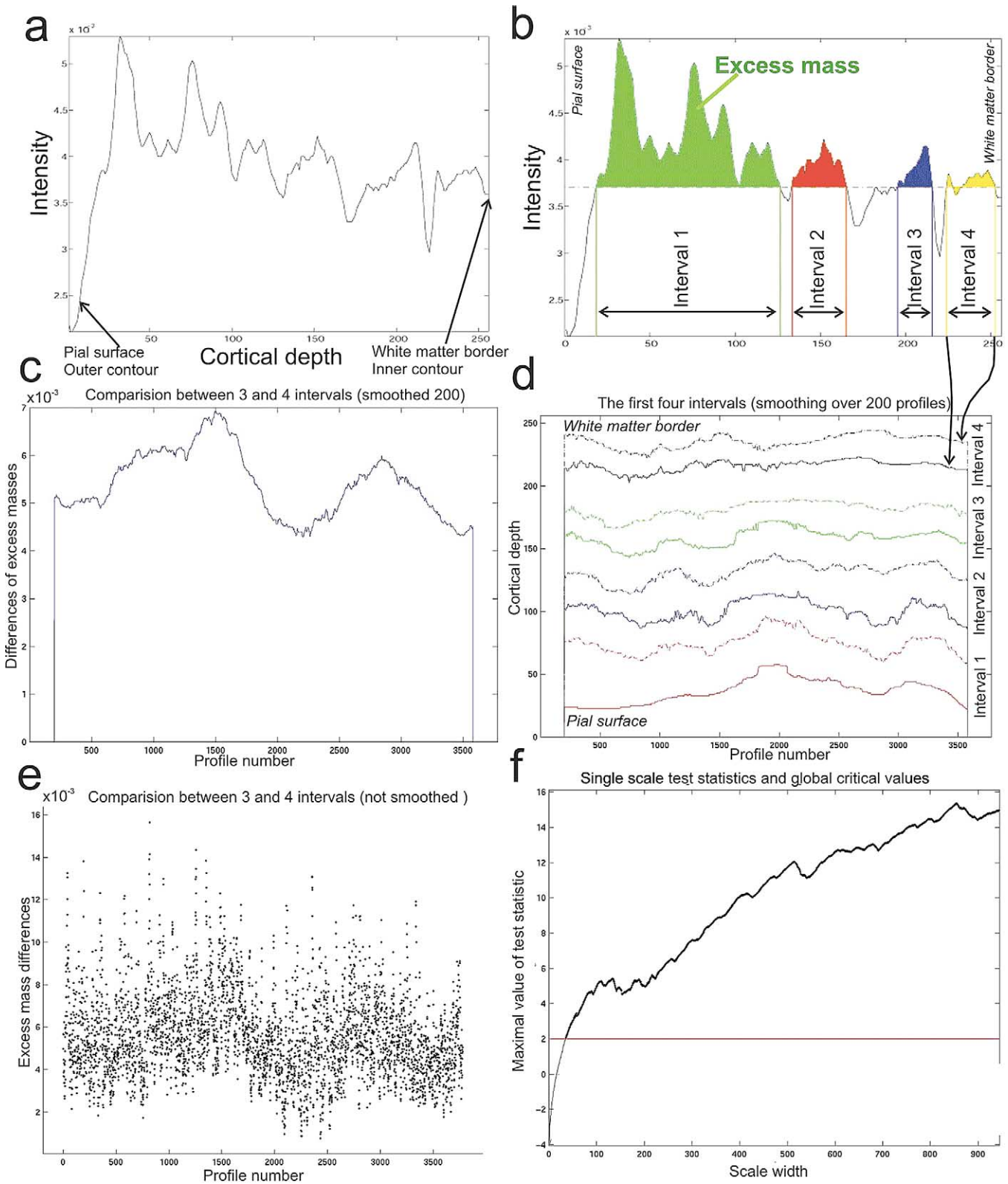

Fig. 2. (a) Single profile of a traverse and (b) the division of the profile into intervals. (c) The differences in excess masses of the interval [3,4] combination over all profiles (1 to 3600) show at which profile regions larger differences appear. (d) Each line marks an interval (cf. subfigure b) running parallel to the cortical surface. The intervals posses an upper border (dashed line) and a lower border (direct line). The upper border of an interval is oriented to the pial surface and the lower border of an interval to the white matter border. The first four intervals that have been used in this excess mass calculation are presented. These are the largest excess masses found within profiles. The four intervals can be considered as an approximation of the real borders of the laminae (cf. subfigure h). (e) This diagram shows all differences of excess masses for all profiles without smoothing. The data are comparable with those of (c), where the same data are smoothed. (f) Single scale test statistic and the global critical value diagram. The red solid line marks the critical value κ, which is determined by a given quantile. The black curve indicates the maximum for the test statistics depending on the scale width. (g) The significant upward and downward interval jumps over all profiles of the interval combination [3,4]. (h) Appropriate profile array.

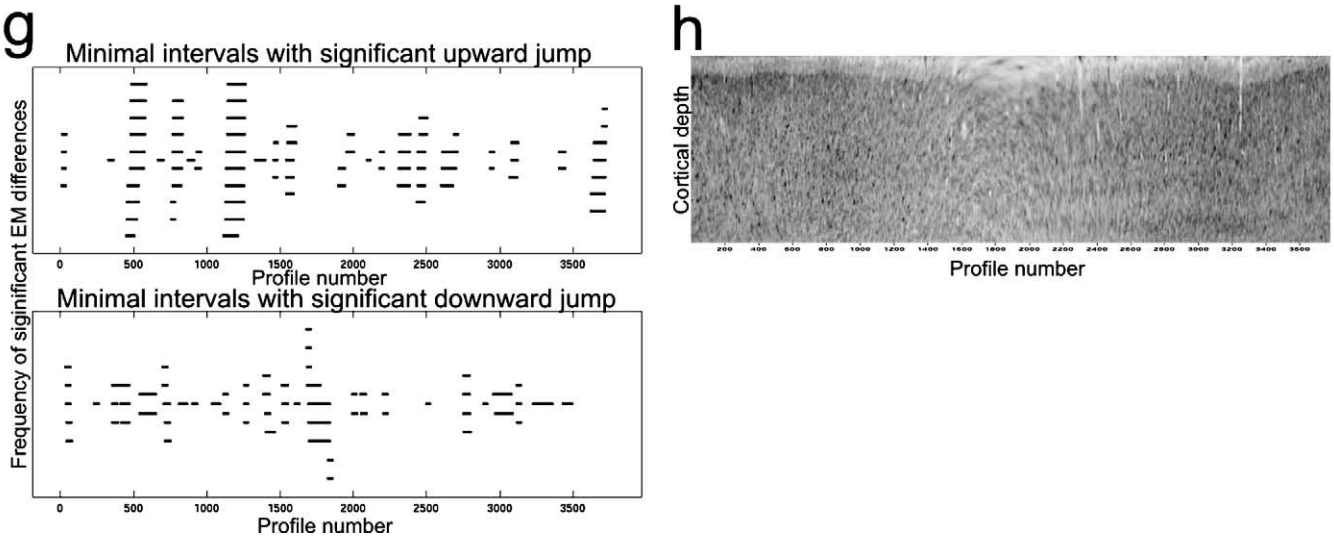

Fig. 2 (*continued*)

lamination pattern at transition regions. A typical feature of the cytoarchitectonic profiles of area 17 are small gray values of lamina IVb, i.e., Vicq d'Azyr stripe, which usually appear as a valley in the profiles. Such a feature is not readily detectable in values that *describe the whole* distribution of gray values in a certain profile. Therefore, this specific structural feature of the distribution cannot be analyzed by a statistical test. This means that complex and very important profile information is reduced solely to single parameters that may be easily affected by the highly curved cerebral cortex (Schmitt and Böhme, 2002). Applying such an approach at long straight segments followed by short less curved or even a single smooth-curved course of a part of the cerebral cortex of the feature vector method leads to reliable results, as shown by Schleicher et al. (1998, 1999). In serial sections, however, we observed much more and stronger folding of the cerebral cortex as well as a high complexity of lamination patterns. This then led us to develop a new method that utilizes the same histologic information that focuses on the intrinsic structural information of the profiles. It is based on the excess mass functional as introduced by Müller and Sawitzki (1991). When applied to a profile of gray levels, these functionals quantify the evidence for a certain number of modes (peaks) and are robust against random noise and spurious peaks. We next analyzed these excess masses to identify a complete series of neighboring profiles in order to find statistically significant abrupt changes. For that purpose, we modified the multiple local rank tests as introduced by Dümbgen (2002). The resulting technique enables transition regions to be detected almost automatically.

Material and method

The histologic sections containing transition regions were obtained from three different brains collected from body donor programs. The specimens were embedded in paraffin wax, sectioned by a sliding microtome into 20-μm-thick sections, and stained with gallocyanin chrom alum (Schmitt and Eggers, 1997b,a), cresyl violet, or the Gallyas-Merker method (Merker, 1983) in order to visualize neurons and other cells in the cerebral cortex. The stained sections were digitized with a high-resolution transparent flatbed scanner (T2500, Agfa) at a resolution of 10.16 μm/pixel. Large neurons like the giant pyramidal neurons within area 4 were easily identified at this resolution (Figs. 7 and 8). In the digitized images, the cerebral cortex was outlined over a region of interest (Fig. 1c). Between, the outer (pial) surface and the inner contour (white matter border), perpendicular traverses (Fig. 1c) were calculated using an electrodynamic model (Schmitt and Böhme, 2002). For each *traverse* (trajectory) a vector, called a *profile*, is generated. This vector contains the gray level values extracted along the corresponding traverse from the outer to the inner contour. Thus the indices of the vector components correspond to cortical depths. Typically such a profile (Figs. 1d and 2a) shows several peaks (modes) and valleys. The size or amplitude and location of the peaks were used by observers to visually distinguish cytoarchitecturally different areas. These profiles were collected in an array (Figs. 1e and 2h) that was imported from the excess mass analysis (EMA) program. Excess masses (Fig. 2b) and their differences (Figs. 2c and d) were calculated and analyzed to determine statistically significant changes (Fig. 2g) of excess mass differences according to the linear rank statistic (LRT) (Fig. 2f) at significance levels of $\alpha = 0.05$ and $\alpha = 0.01$.

At this point a brief overview over EMA is given. For a more detailed description of the mathematics and algorithms we refer to the appendix.

As mentioned before, profiles exhibit several local peaks or, in statistical terms, modes. Over a series of profiles these modes form the lamination pattern of the cortical area in

question. Thus, changes in the distinctiveness and number of the modes are an indicator of transition regions. In order to quantify such phenomena, we use a modification of the so-called *excess mass functional* (Müller and Sawitzki, 1991). For a single profile such a functional measures areas under the profile curve exceeding certain thresholds. For one particular threshold λ, a maximal set of consecutive indices such that the corresponding gray level values exceed λ is called a λ cluster (Fig. 2b). As the threshold increased, the λ clusters concentrated on the modes of the profile. Note that random errors in the data lead to many local peaks in a profile. The *restricted excess mass functional* restricts the number of λ clusters that contribute to the excess mass to an integer M; only the M largest ones are considered. The difference between the excess masses for two numbers $M < \tilde{M}$ was computed for several equidistant thresholds λ ranging from 0 to the maximum gray level value of the profile. The maximum of these differences was called the *excess difference* for $(M, \tilde{M})$. Note that this difference is close to zero if the profile has at most M strong plus some spurious modes. The excess difference measures to what extend $\tilde{M}$ modes seem more appropriate than M modes.

Changes in the excess difference over a series of consecutive profiles indicated a change in the distribution of modes. For instance, imagine a region with a sudden change from two to three laminae. Then the excess difference for $M = 2$ and $\tilde{M} > 2$ will increase. The strength of such changes is quantified via a local linear rank statistic (Dümbgen, 2002). Each local rank statistic corresponds to a certain subarray of profiles, and we consider all possible subarrays comprising up to m consecutive profiles simultaneously. Therefore, we apply a multiple test procedure in order to detect and localize significant changes. The multiple test does not use a Bonferroni or Bonferroni–Holm adjustment of P values. Instead it is based on a certain multiscale statistic as described in the Appendix.

To conclude this description, the EMA consists of two steps. In the first step the excess differences are computed for a number of different pairs $(M, \tilde{M})$. In the second step these excess differences are examined for significant sudden changes by means of multiple local rank tests (MLRT). Since there are many possible pairs $(M, \tilde{M})$, we developed a graphical tool to combine all results and display them in one diagram, called an *interval assay* (Fig. 1f). Each row corresponds to a certain pair $(M, \tilde{M})$. The left and right plots depict significant increases and decreases in the excess differences, respectively. The horizontal axis corresponds to the profile numbers. Profiles outside any region with significant changes are color-coded blue. Otherwise they are coded from green to red, depending on the strength of detected trends. With the aid of these interval assays we are able to find those jumps which are robust in the sense of a repetitive occurrence over different pairs $(M, \tilde{M})$.

The EMA was conducted on five examples in order to test the method in transition regions of cortices with varying lamination patterns and in serial directly adjacent sections: (Example 1) The transition region between Brodmann areas 18 and 17 in serial sections 116 to 123 of the left and right hemisphere of the occipital lobe (Figs. 4 and 5); staining, gallocyanin chrom alum; section thickness, 20 μm. (Example 2) The transition region between Brodmann areas 4, 3a, 3b, and 1 (Fig. 4); staining; Gallyas–Merker; section thickness, 20 μm. (Example 3) The transition region between Brodmann areas 4 and 6 (Fig. 7); staining, cresyl violet stain; section thickness, 20 μm. (Example 4) The transition region between Brodmann areas 3b and 3a, 4, 6a (6aβ) and 6p (6aα) (Fig. 8); staining, Gallyas–Merker; section thickness, 20 μm. (Example 5) The transition region between Brodmann areas 4a and 4p (Figs. 9 and 10); staining; Gallyas–Merker; section thickness, 20 μm.

EMA and statistical analysis were realized via Matlab 6.1 (Mathworks). The scripts were compiled on a Sun Fire 15K (Solaris 8) machine which is a cache coherent nonunified memory access parallel computer with 72 UltraSPARC-III Cu 900 MHz processors and 72 GB of memory and Intel PIII machines operating under Linux (2.2.4).

Results

Example 1: Transition of area 18 to 17

In the first example, section number 121 of the right occipital lobe (Fig. 3) from the series 116 to 123 was investigated in order to present the analysis in greater detail. In this section, EMA was conducted to search for the transition region between Brodmann areas 18 and 17. The original image is shown in Fig. 3a and the traverses in Fig. 3b. In the profile image (Fig. 3c), the transition region t_1 at traverse positions 300 and $t_2 = 1900$ is obvious. Up- and downward jump interval assays at a significance level of $\alpha = 0.01$ and a frame size of $m = 150$ are documented in Figs. 3d and e. We expected significant upward jumps at t_1 because the number of modalities at this interval typically increases from area 18 to area 17 (indicated by an arrow in Fig. 3d). At traverse position 1900 (Fig. 3e), the decrease of modalities respective to lamination was found by EMA.

The EMA results of the profiles (Fig. 4, right) of sections 116 to 123 of the left and right occipital lobes (Fig. 4, left) are summarized in Fig. 5. The significant up- and downward jump patterns of all interval combinations of the excess masses exhibited the same structures as those demonstrated by the EMA result of section 121 of the right occipital lobe. Upon examining of the left occipital lobe, we found that t_1 lies between traverses 200 and 300 and t_2 between traverses 1900 and 2100. In comparing the upward jumps that indicate t_1, we found significant changes between traverses 200 and 300. However, fewer significant jumps were detected in section 119. The second transition region (t_2), from areas 17 to 18, was detected as well. Interestingly, however, we also detected a very strong convexity blurring the lamination of

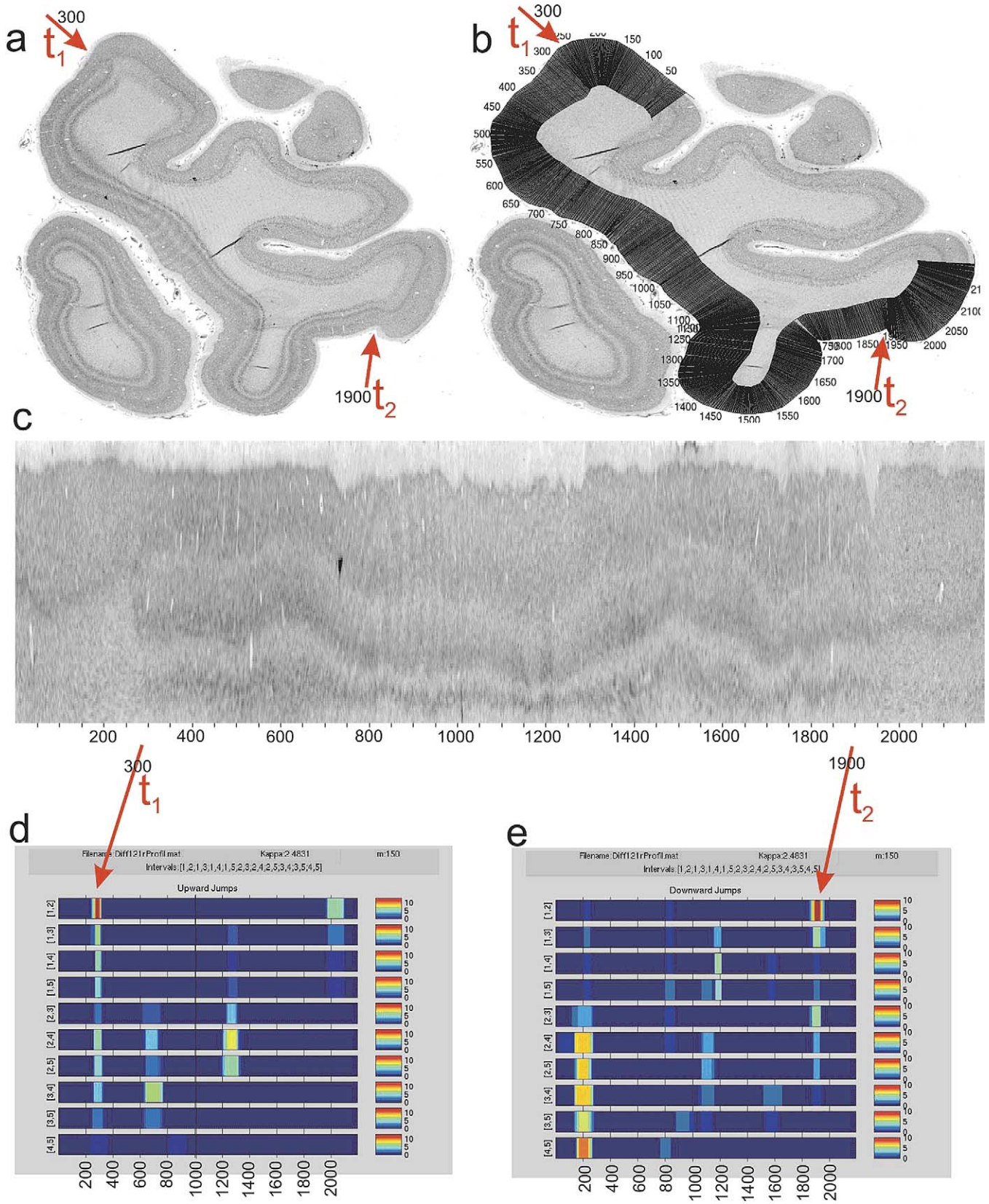

Fig. 3. The images and diagrams shown here are enlargements and parts of Fig. 4. (a) Section 121 through the right occipital lobe is presented as a flatbed scan image and as (b) the associated traverse image. (c) The resulting profile array. EMA interval arrays for significant upward jumps (d) and downward jumps (e) are shown, the arrows indicating the corresponding position of the profile array and the interval array. The downward jump diagram shows also a significant excess mass change of the interval combinations from [2,3] to [4,5]. However, this change must be rejected for two reasons. First, the lamination increases from area 18 to 17 around profile position 300 (found by the upward jumps) and not 200 (found by downward jumps). Second, the change in the downward diagram is blurred; however, we expect a sharp change of lamination, which is obviously detectable in (a) and (c). This means that the investigator must analyze the upward and downward diagrams critically in relation to the profile data and to the original high-resolution image or mapping.

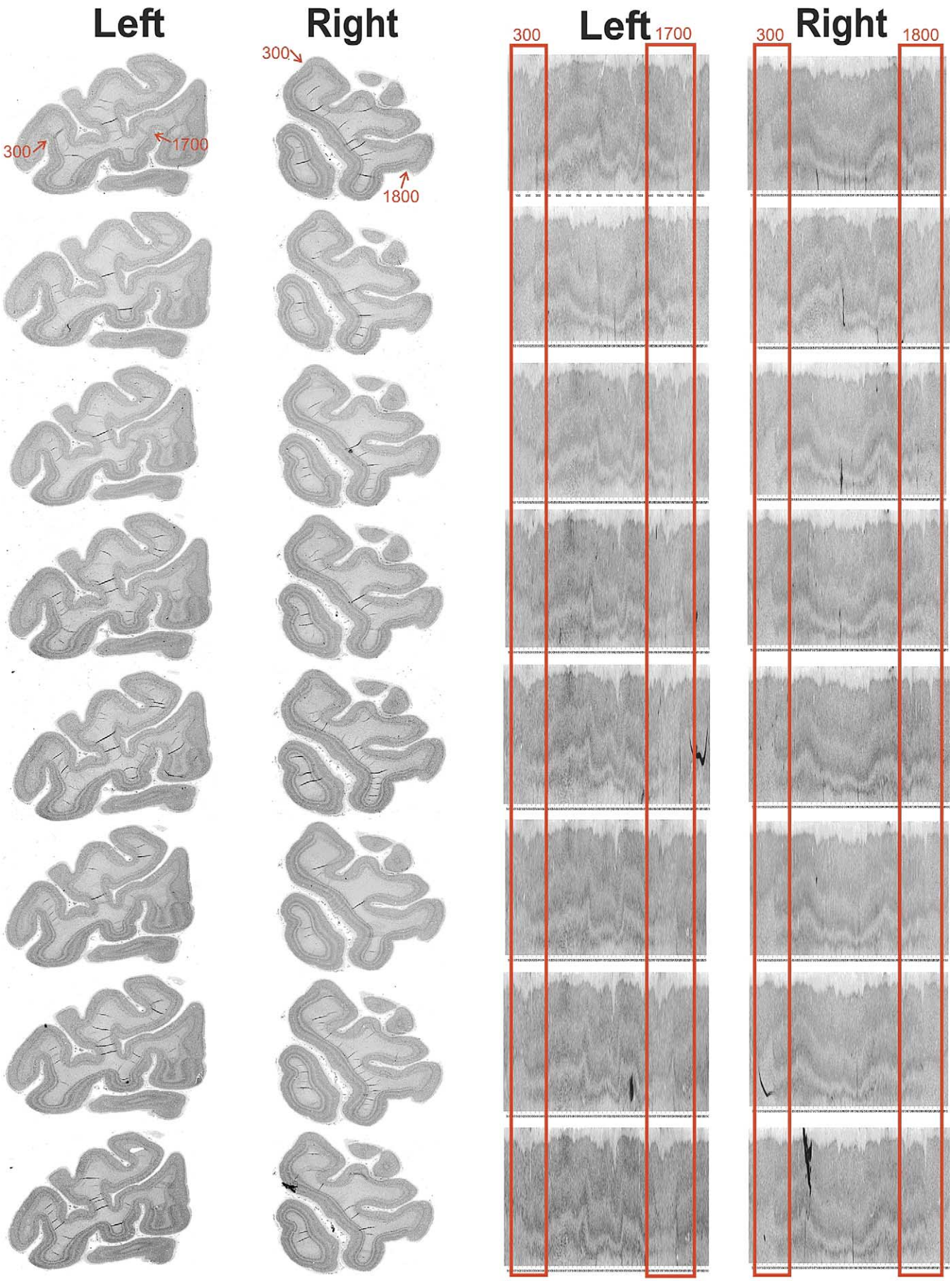

Fig. 4. In this figure serial sections through the occipital lobes and their profile arrays are summarized. The transition regions in the left and right hemispheres are indicated in the upper diagrams by profile numbers as well as in the profile arrays (red boxes). The profile numbers around the transition regions are highlighted because exactly these profile positions were detected by EMA and are presented in the interval diagrams in Fig. 5.

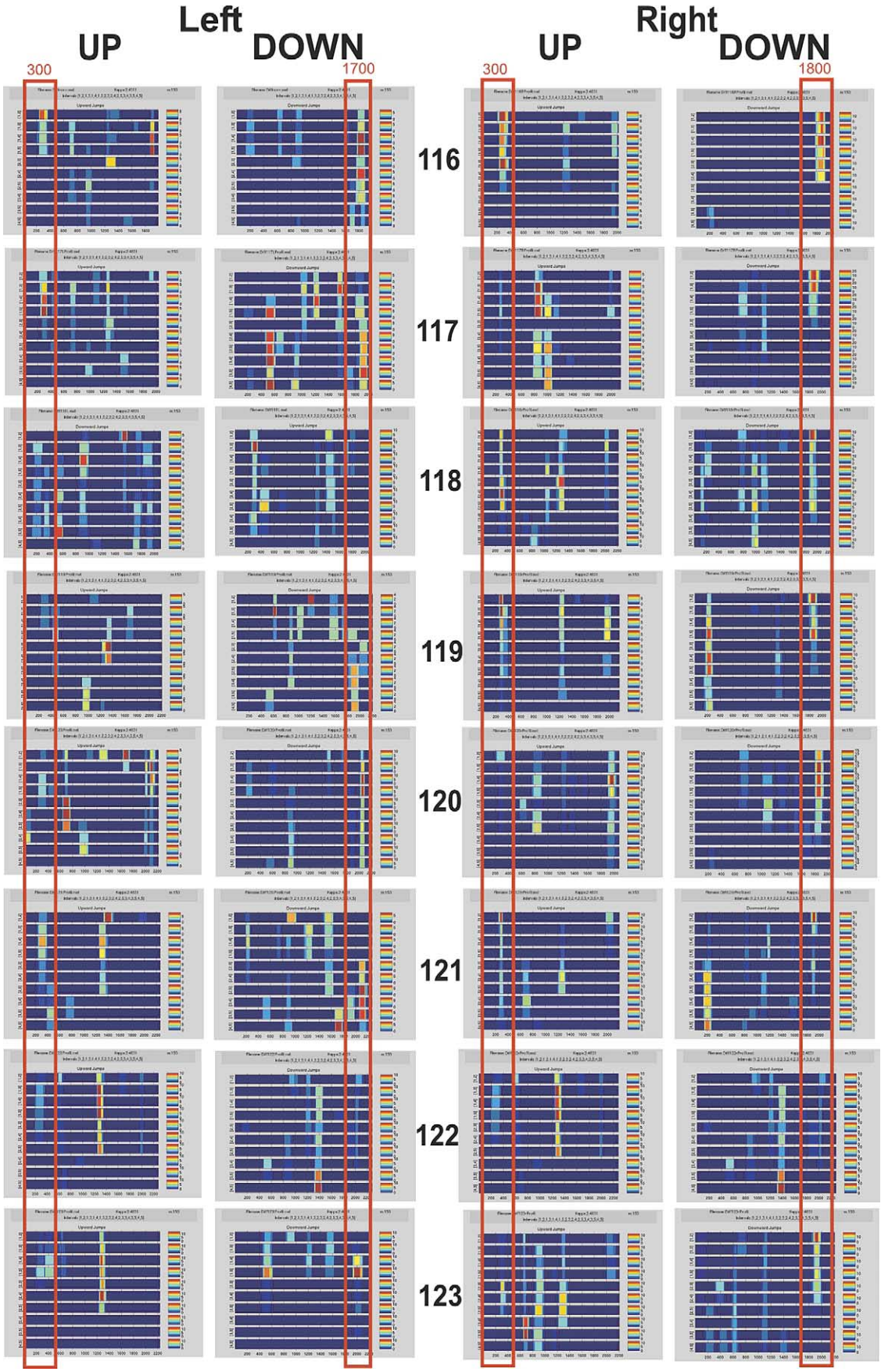

Fig. 5. The interval arrays corresponding to significant up and down jumps are presented in the same order as used in Fig. 4. The numbers of the histologic sections are printed in the middle of this figure. Around profile position 300 there are significant upward jumps in the right hemisphere indicating the transition from area 18 to 17. The comparable upward jumps can be detected in the sections through the left hemisphere as well. The significant downward jumps indicating the transition from area 17 to 18 lie around profile position 1700 in the left hemisphere and around 1800 in the right.

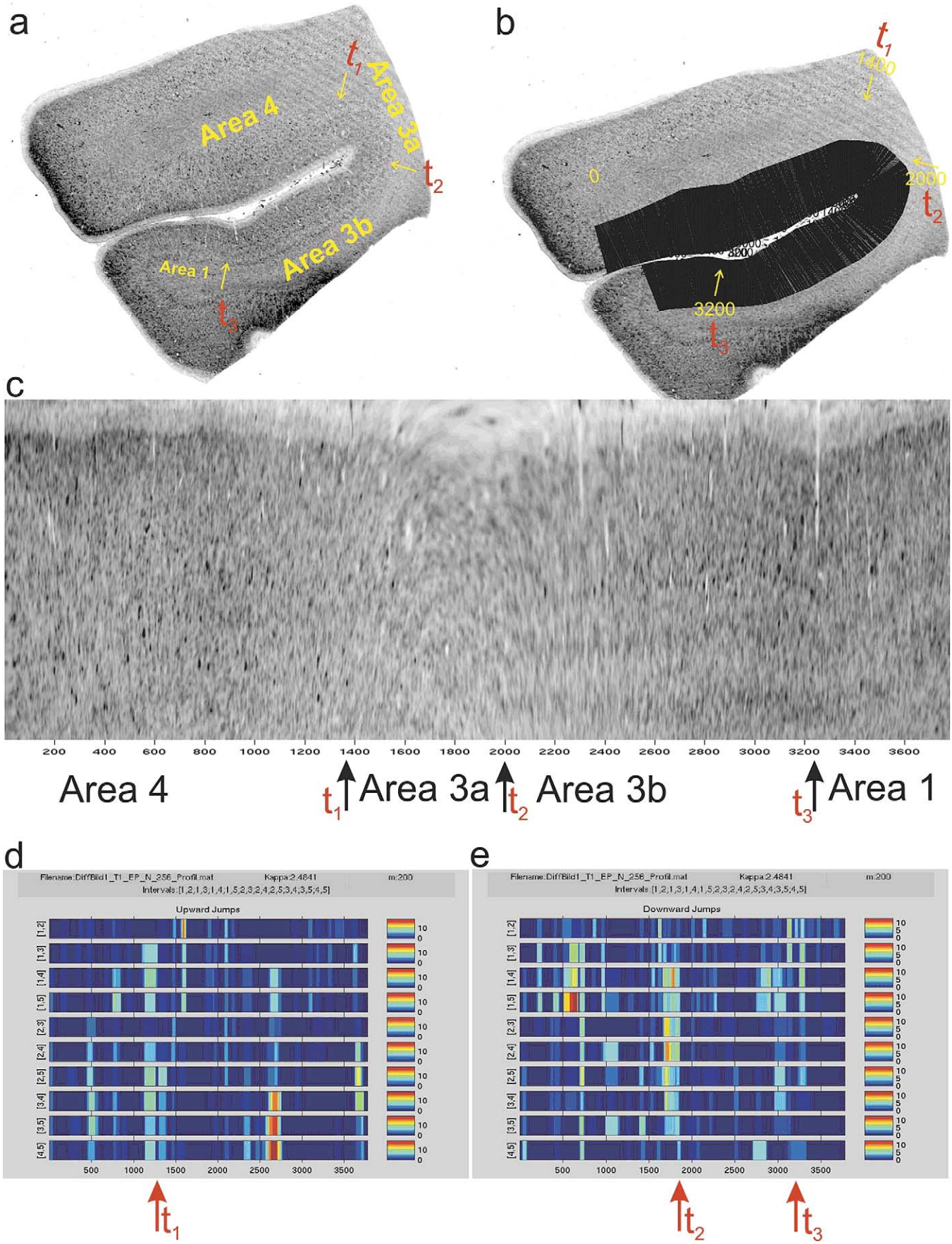

Fig. 6. Flatbed scanned section (a) containing areas 1, 3a, 3b, and 4. The respective traverse image is shown in (b) and the profile array with the areas and transition regions t_1 to t_3 in (c). The significant upward jumps for the transition region between areas 4 and 3a is located around profile position 1400. This pattern change has been detected as an upward jump (a) because the numbers of layers increase from area 4 to 3a. In the downward jump diagram (e) significant changes were found around profile positions 1800 and 3200.

area 17 just before area 18. The transition region was detected in this transient zone, too.

Example 2: Transitions between areas 4, 3a, 3b, and 1

The second example shows the cytoarchitectural situation around the central sulcus. An experienced observer can easily distinguish Brodmann areas 3 and 4 in the FBS image (Fig. 6a). The transition regions (t_1 to t_3) are indicated by arrows in Fig. 6a and in the corresponding traverse image (Fig. 6b). The profile array shows a nonlinear mapping phenomenon within strong concavities or sulcus basins (also, not shown here, at convexities or sulcus caps). The arrows in the interval assay (Figs. 6d and e) are located around the same positions as those shown in (Figs. 6a–c). The transition region between areas 4 and 3a is exactly located between profile positions 1300 and 1400 according to Fig. 6d. This transition region location corresponds with the expected transition region of the histologic image in Fig. 6a. The transition region of areas 3a and 3b is found around profile position 2000, a position that coincides with the expected region in the histologic image (Fig. 6a). Finally, the transition of area 3b to area 1 was detected around profile position 3200, again meeting expectations of location as presented in the histologic image (Fig. 6a). In short, EMA found the transition regions comparable to those identified by an experienced observer.

Example 3: Transition of area 4 to 6

In our third example, we demonstrate detection of the transition region between Brodmann areas 4 and 6. In the FBS image (Fig. 7a), Brodmann areas 4 and 6 can be distinguished readily due to the registration of giant pyramidal neurons afforded by the high-resolution flatbed scanner. The transition region was expected to be within profiles 2600 to 3200. EMA marked this region at $\alpha = 0.01$ by applying the JumpNTrends option and utilizing a frame size of 400. Because this is a quite wide range, the region of interest (ROI) was reduced around traverses 2000 to 4000, as indicated by a black frame in Fig. 7d. After repeating EMA in this ROI, a significant upward jump of excess mass was detected exactly around traverse position 3000 (red arrow). In the interval assay of the downward jumps, another cluster of significant intervals was found around traverse position 6000. Sarkissov et al. (1955) subdivided area 6 into a posterior part (6p) and an anterior part (6a) (i.e., 6aβ and 6aα; Vogt and Vogt, 1919). The latter subdivision, as described, lies close to the superior frontal sulcus. The significant downward jump just behind the precentral sulcus close to the convexity of the precentral gyrus may be an indication of 6p to 6a transition.

Example 4: Transition of areas 3b, 3a, 4, 6p, and 6a

This most complex example (Fig. 8) consists of a profile array containing almost 10,800 profiles, each with a normalized length of 256. In the profile array (Fig. 8c) areas 3, 4, and 6 can be distinguished, as indicated by the respective arrows. Four transition regions, t_1–t_4, delineate the borders separating areas 3b, 3a, 4, 6p, and 6a. There are two transition regions expected around Brodmann areas 3 to 4 (t_1) and Brodmann areas 4 to 6 (t_2). As indicated by arrows in the interval assays, these regions can be detected at the expected positions (Fig. 8d). Transition regions t_1 to t_3 show significant excess mass jumps in the downward interval assays at positions 1400, 3200, and 5200. Region t_4 was detected by EMA in the upward interval assay around position 8200. Because t_2 and t_3 are not so explicit, the region in between positions 2500 and 6500 was enlarged and tested with frame sizes $m = 150$ and $m = 400$. By using frame size $m = 400$ and a significance level of 0.01, we detected the expected transition region; t_2 was detected in interval combinations [2,4] to [4,5] and t_3 in interval combinations [1,3] to [1,5].

Example 5: Transition of areas 4p and 4a

An ROI in the section of the previous example (Fig. 8a) was defined over nine different specimens (directly adjacent serial sections) (Fig. 10). Within these ROI traverses were generated using an intertraverse distance of one pixel. The profile array was analyzed by EMA, incorporating five intervals, JumpNTrends mode, a frame size $m = 500$, and a level of significance of $\alpha = 0.01$. The frame size or length of intervals m was confirmed by multiscale analysis, as shown in Fig. 9. A transition region of area 4p to 4a was expected around profile position 1500. In an enlarged view of the profile array, this expected and the subsequently demonstrated transition region is marked. Area 4a is characterized by larger sizes of neurons and a larger density of neurons in lamina III. These results show clearly that EMA and MLRT methods lead to reproducible results at similar locations in directly adjacent serial sections.

Fig. 7. (a) Scanned section containing area 4 (blue) and 6 (red), (b) representing the traverse image and (c) the resulting profile array. In EMA of all profiles (d) suspicious zones were detected. However, it is unclear which interval jumps must be preferred and which have to be discarded. Therefore, EMA was used to focus on details (black frames with arrows) within intervals [1,4] to [4,5], one window (upward jumps) of profiles between profiles 2000 and 4200 and a second window (downward jumps) between profiles 3500 and 5500. The resulting interval arrays are shown in (e). EMA detected the expected transition between areas 4 and 6 as indicated by the red arrow in the upward jump diagram and within area 6 a significant downward jump around profile position 6000, which may indicate the transition from areas 6p to 6a. Note that the giant pyramidal neurons are clearly visible as black dots in the profile arrays and in the scanned section (a cluster of four giant pyramidal neurons is marked by the yellow circle), which has a resolution of 5150 × 2580 pixels. Because such a large image must be interpolated for reproduction some blurring effects occur.

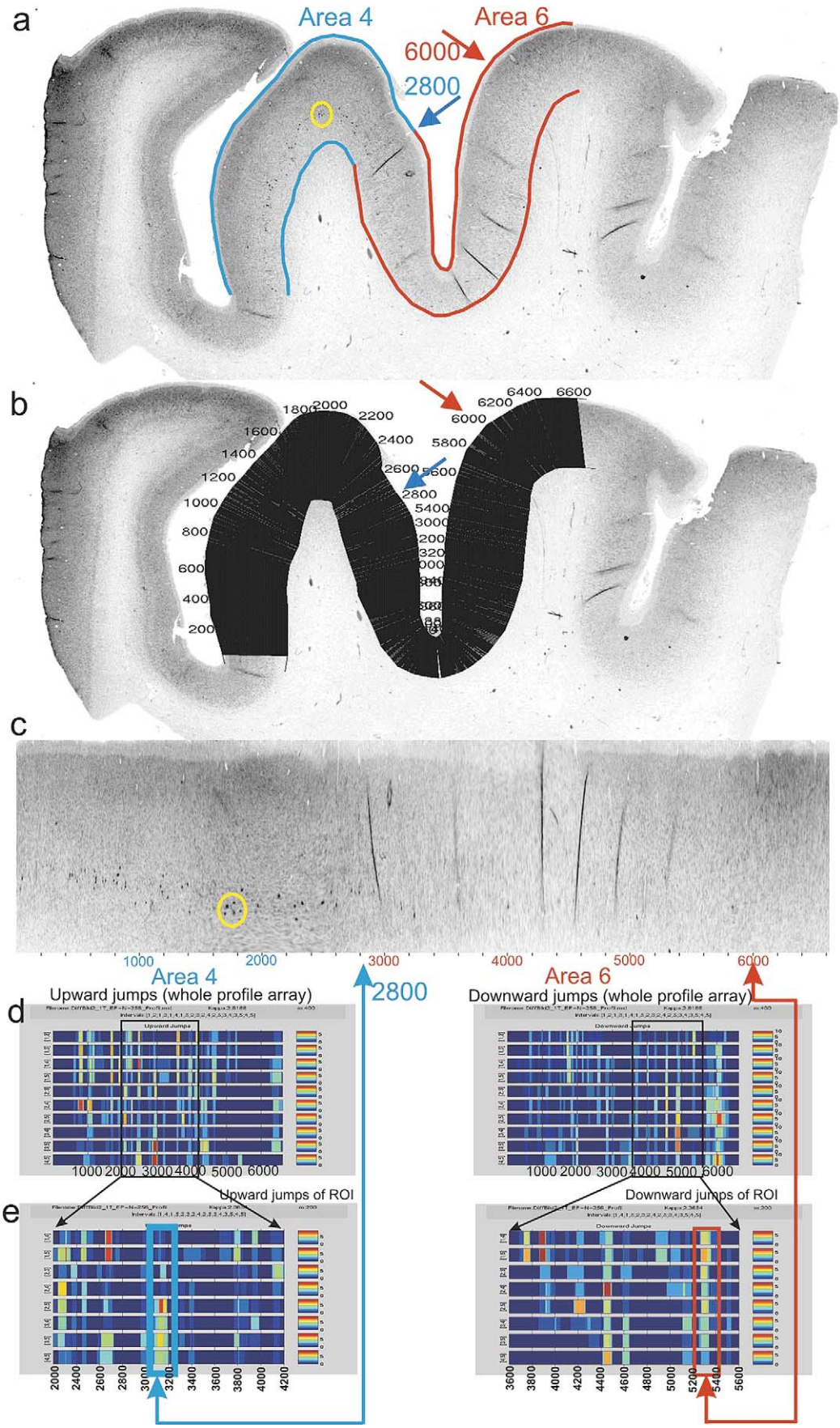
a
Area 4
Area 6
6000
2800
b
1800 2000 2200 1600 1400 1200 1000 800 600 400 200
6400 6600 6200 6000 2400 5800 2600 5600 2800 5400 3000 200 320
c
1000 2000 3000 4000 5000 6000
Area 4
Upward jumps (whole profile array)
2800
Area 6
Downward jumps (whole profile array)
d
1000 2000 3000 4000 5000 6000
Upward jumps of ROI
Downward jumps of ROI
e
2000 2400 2600 2800 3000 3200 3400 3600 3800 4000 4200
3600 3800 4000 4200 4400 4600 4800 5000 5200 5400 5600

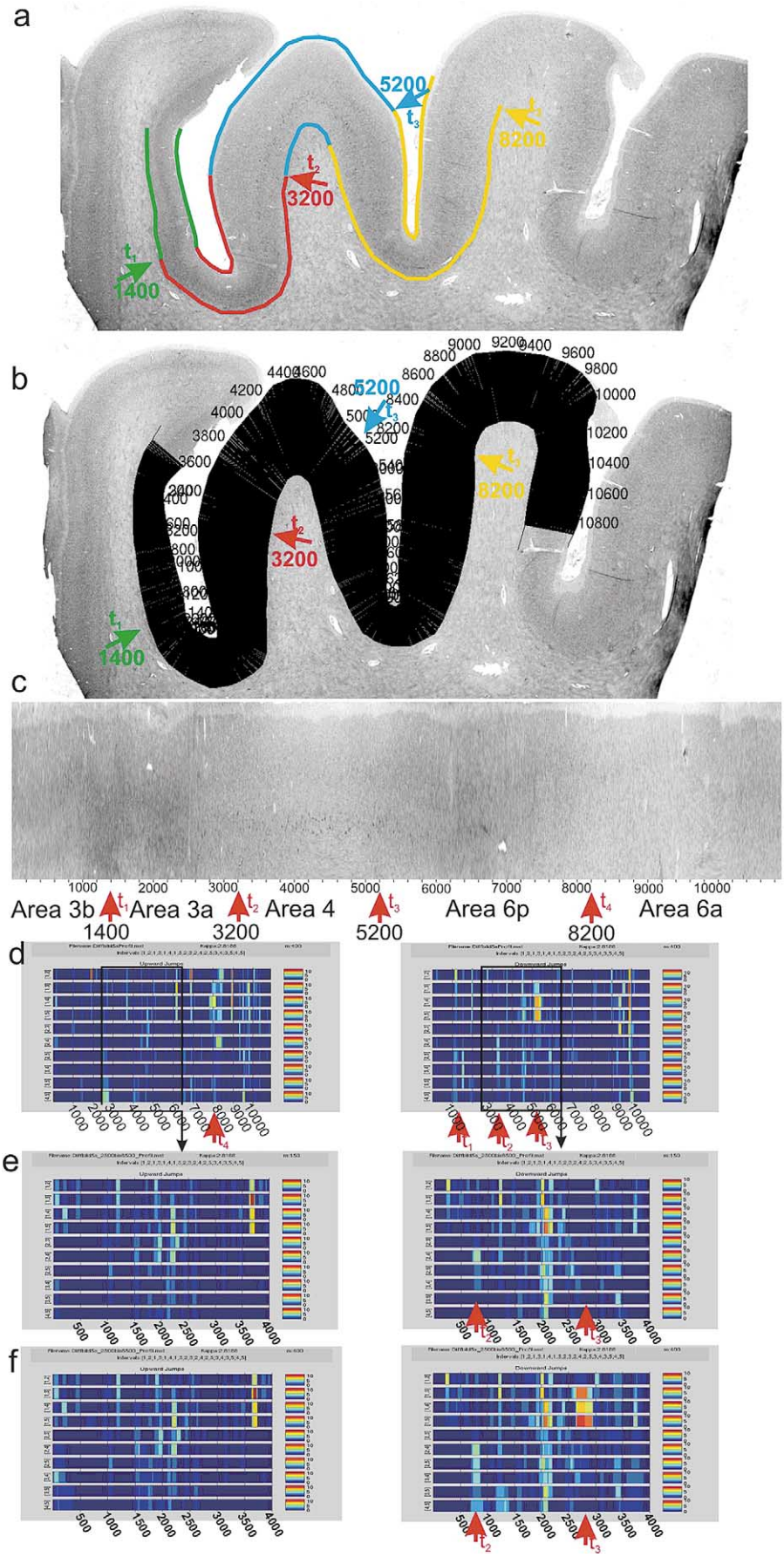
a
5200
8200
3200
1400
b
5200
8200
3200
1400
c
1000 2000 3000 4000 5000 6000 7000 8000 9000 10000
Area 3b
Area 3a
Area 4
Area 6p
Area 6a
1400
3200
5200
8200
d
e
f

Some comments on m

The MLRT involves the parameter *m*, the maximal length of intervals to be considered. This parameter is used for reducing the computation time. However, *m* should be chosen according to the expected size of transition areas. This aspect is illustrated in Figs. 9 and 11. For each *m* in a certain range we depict an interval assay as one bar. Strong structural changes are readily apparent for small *m* values, but the identification of weak and/or gradual transitions over a wider transition region requires larger values of *m.*

Discussion

The idea of statistically based detection of transition regions was introduced first by Schleicher et al. (1987) and further improved thereafter (Schleicher et al., 1998). It subsequently was shown by Amunts et al. (2000, 1999a, 1999b, 1998) and Geyer et al. (1996, 1999) that a statistically significant change of lamination pattern coincides with cytoarchitecturally defined changes in transition regions. The comparison of feature vectors derived from the distribution of image intensities or gray level indices (Schleicher et al., 1978) of profiles is an encouraging starting point for further development of the statistically based analysis of profiles. Hotelling's T^2 test (Bartels, 1981) with Bonferroni adjustment of the *P* values for multiple comparisons (Dunn, 1961) analyzes the Mahalanobis distances (Mahalanobis et al., 1949) of adjacent blocks of profile feature vectors. Alterations of the macroscopic curvature of the cerebral cortex may lead to false positive significances, especially at those locations where the straight path of the border of the cortex turns into an inflexion. Such alterations of the geometry inevitably influence the statistical properties of a profile and, consequently, extracted features. We attempted to mitigate such effects by applying a new approach to generating traverses (Schmitt and Böhme, 2002), developing a new statistical technique for determining and analyzing traverses and transitional regions. EMA analyzes the pattern of intensity distributions or profiles, promising a pivotal analytical difference to and improvement from the above methods in calculating prime and derivative moments of profiles (Schleicher et al., 2000). Structural changes in the lamination pattern may be detected by observers per the pattern of changes of cell densities (Roland and Zilles, 1998), but such observations may not replace or supplant the accuracy of such information about the cell density shape with the density moments. Even if feature vectors contain many standard parameters that characterize a distribution, such as mean intensity, standard deviation, skewness, kurtosis, and the gravity center of the cortical depth (Schleicher et al., 2000) they do not make use of the most important information from a profile: its modality or pattern of profile peaks and valleys. In different examples, it is shown here that EMA detects nonobvious structural changes of the lamination pattern (areas 4 to 3b and areas 3b to 3a) as well as obviously strong structural jumps.

Yet heretofore, there has existed no algorithm that is *completely* observer-independent for the detection of all kinds of statistically significant lamination changes. For EMA the user has to specify some parameters, such as a pair $(M, \tilde{M})$ of interval numbers, the frame size *m*, the significance level, the detection mode (Jump, JumpNTrends), and the start and stop within the profile array. However, by using these parameters properly, one can optimize EMA to more precisely determine specific problems in lamination analysis. Therefore, excess mass analysis is a detection and visualization tool for investigating complex data arrays. It is well known that EMA cannot differentiate between or among artifacts like folding or staining inhomogeneities and real changes in lamination patterns; it is indispensable that an observer evaluate the results critically and compare those locations of significant changes of the interval arrays with the images of the profile arrays in order to exclude the influence of artifacts (Example 1). If artifacts are excluded and unexpected significant interval jumps appear, then jumps must be confirmed or rejected by analyzing serial sections. We accomplished this in our study (see Figs. 4 and 10). By analyzing various series of profile arrays, we are able to confirm findings, i.e., a subdivision of area 4 into areas 4p and 4a (Zilles et al., 1995; Roland and Zilles, 1996; Geyer et al., 1996; Fink et al., 1997; Naito et al., 1999, 2000; Hilbig et al., 2001; Johansen-Berg and Matthews, 2002), that cannot be otherwise detected easily. The same holds true for the transitions of areas 3a to 3b (Geyer et al., 1999) and areas 17 to 18 (Amunts et al., 2000) that were revealed via the EMA technique.

Furthermore, we did get a hint of the number of layers increasing (upward jumps showed significances) or/and decreasing (downward jumps showed significances) at the transition regions.

The orthogonal sections through the cerebral cortex were quasi-orthogonal, only. Yet, within the sectioning process it

Fig. 8. This is a section following the one shown in Fig. 7a. (a) The last one expatiated in the second example this time, however, stained according to Merker (1983). The (b) traverse path has been elongated with regard to the path in the last example. The areas and transition regions are marked in the profile array (c), which consists of about 11,000 profiles. The experts expect almost four different transition regions, as indicated by t_1 to t_4, because, as mentioned in the last example, significant upward and downward jumps are less clearly pronounced. Therefore, the ability of EMA to set parameters in order to focus on ROIs was applied. Using a frame size of $m = 150$, significant jumps indicating the transitions t_2 and t_3 were not detected. However, testing the same ROI of the profile array again with an frame size of $m = 400$ (f), significant downward jumps at position 3200 (t_2) for interval combinations [2,4] to [4,5] and at position 5200 (t_3) for interval combinations [1,3] to [1,5] were detected. This optimal *m* of 400 was determined by exploring *m* over different scales (multiscale exploration), as documented in Fig. 9.

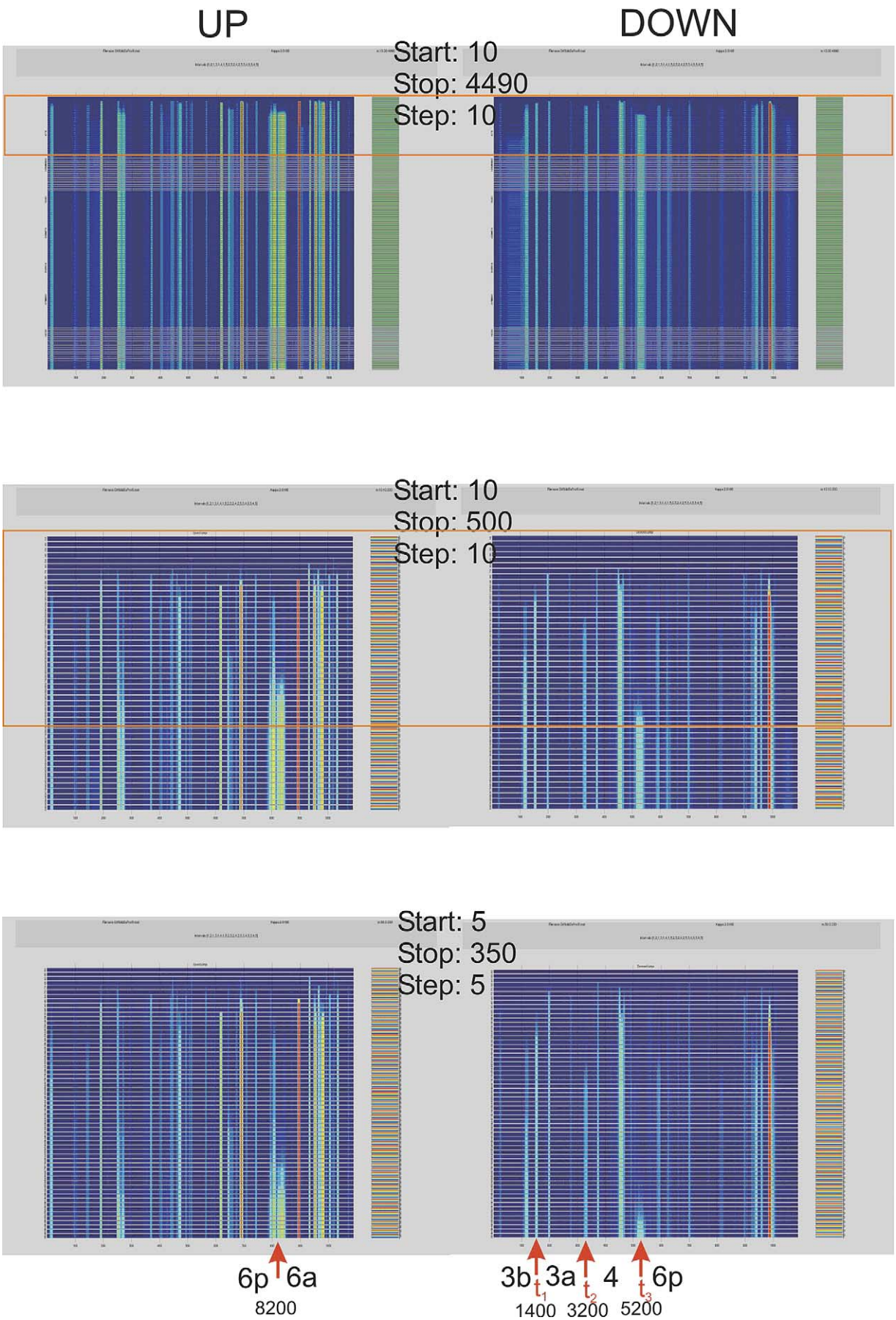

Fig. 9. Multiscale exploration of the example shown in Fig. 8. The left and right diagrams on top represent the summed interval combinations from $m = 10$ to $m = 4490$ with m steps of 10. The rectangle indicates the search zone of interest (SOI), which lies between an m of 10 and 500. The result of the exploration of this zone is shown in both diagrams in the middle. The next SOI lies between $m = 10$ and $m = 350$ and it is explored by m steps of 5. Using this larger resolution, all four transition regions which were expected according to Fig. 8 were found.

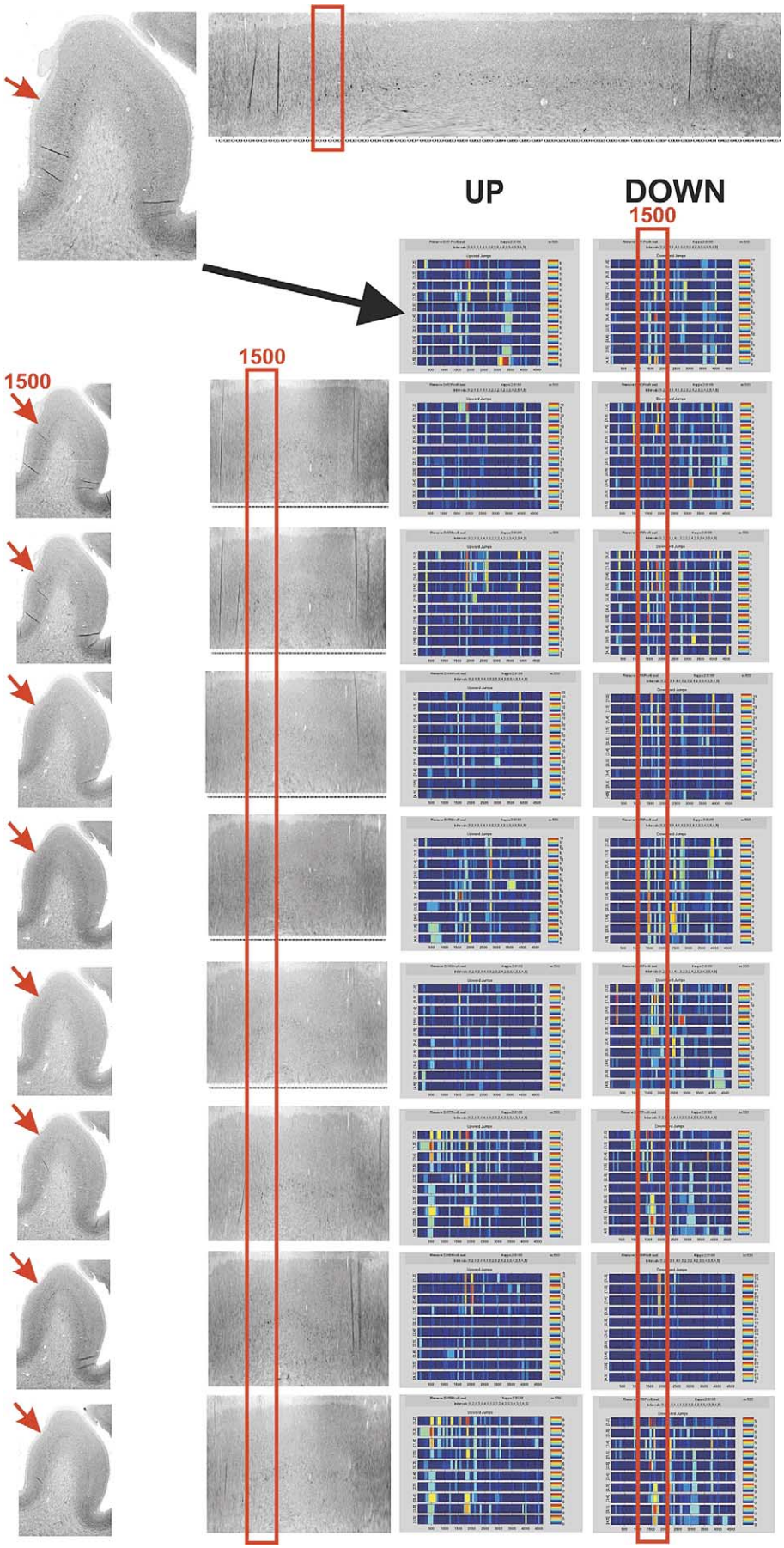

Fig. 10. In serial section profile analysis of the primary motor cortex by EMA using an optimal *m* of 500, as determined by multiscale analysis in Fig. 11, a significant downward jump of interval combinations [1,4] to [3,4] was found in all profiles. This is a statistically significant finding which must be considered evidence for a transition region in area 4, which subdivides the primary motor cortex into areas 4p and 4a.

UP
Start: 10
Stop:2210
Step 100

DOWN
Start: 10
Stop:2210
Step 100

UP
Start: 10
Stop: 500
Step 10

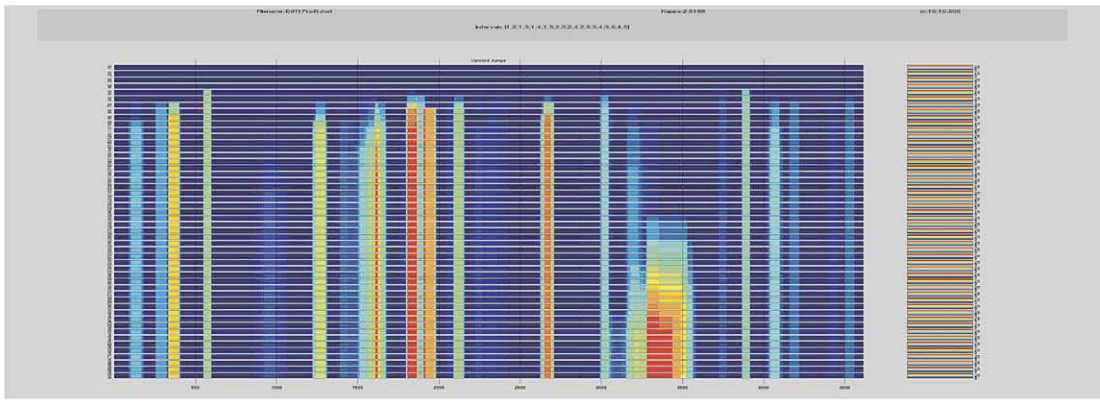

DOWN
Start: 10
Stop: 500
Step 10

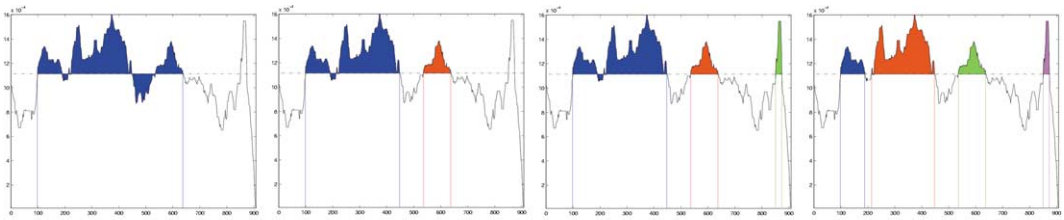

(a) $M = 1$ (b) $M = 2$ (c) $M = 3$ (d) $M = 4$

Fig. 12. This figure illustrates the lemma for an arbitrary λ. As the number of intervals increases a new interval is added or an existing interval is split.

is solely possible to produce sections which are as orthogonal as possible. Optimal orientation cannot be assured in each section. This may influence the detection of transition regions, and it is important that the algorithm used be robust enough (Schmitt and Böhme, 2002) in order to find significant changes in the lamination pattern in and around blurred profile arrays. A further problem was observed when strong sulcus basins and gyrus crowns were scanned by the traverse generator. In such ROIs of the profile arrays, blurring increases nonlinearly (Fig. 6) in the direction of the white matter border at gyrus crowns and vice versa at the sulcus wall. Interestingly, Amunts et al. (2000) found significant changes in their analysis of profiles at some gyrus crowns and sulcus basins, indicating the fringe area and the border tuft within the transition region of area 17 to 18. Such an apparent significant change of adjacent profiles also could be the result of an increase in geometric differences around inflexion points (e.g., strong increase or decrease of gradients) within the cortical path.

To adapt profiles locally independent of their position and geometry over the whole course of the scanned cerebral cortex, new techniques for correcting blurring in profile arrays have to be developed. The EMA approach seems to be the first technique in lamination analysis of the cerebral cortex that uses the information contributed by the pattern of a profile.

A final remark should be given about 1D discrete fast Fourier transformation (FFT) (Peters and Williams, 1998) and and wavelet (Blatter, 1998) analysis of profiles. The disadvantage of FFT is that spatial information which is necessary for the localization of transition regions in profile arrays is lost. Applying wavelet analysis, we recovered spatial and frequency information on each profile of the profile array. However, the individual pattern in the search window was not preserved, and it was not obvious which features of the wavelet transforms should be analyzed. With respect to these transformations their results are distributions that can be analyzed by the EMA.

However, we applied and developed EMA in a first approach on the original data of profiles and not on transformations which may have been accompanied by other problems. The excess differences were analyzed statistically by means of a multiple linear rank test in which the local ranks were entered into the test statistics linearly. An advantage of this approach is that the explicit computation of the MLRT is feasible. In principle, one could replace the Wilcoxon score function with nonlinear functions, such as the Fisher-Yates or the van der Waerden score function (Pratt and Gibbons, 1981). But such an approach would increase the computational efforts drastically, whereas the gain in sensitivity would be rather small. In addition, using a nonlinear and unbounded score function would increase the influence often erroneous profiles that may be caused by artifacts.

The first derivative of cortical fingerprints (Schleicher et al., 1998, 1999) has not been studied so far by EMA. This may be of interest in cases of cortical laminations where wide layers with slight neuronal densities appear. However, it seems unlikely that analyzing the first derivatives of cortical fingerprints investigated here would produce different results.

The effect of inflexions of the cortical path with relatively short profile lengths around straight walls and relatively long profile lengths between the crown and fundus of a gyrus may be reduced by nonlinear unfolding techniques (Jouandet et al., 1989; Carman et al., 1995; Manceaux-Demiau et al., 1998; Fischl et al., 1999; Xu et al., 1999) which we did not apply in this study.

Summary

The EMA technique is introduced here for the first time for profile analysis of cytoarchitectonic lamination patterns. As tested in cortices with a wide range of different lamination patterns, EMA is obviously robust with respect to

Fig. 11. Multiscale exploration of serial sections of the primary motor cortex. The left and right diagrams at the top represent the summed interval combinations from $m = 10$ to $m = 4490$ with m steps of 10. The rectangle indicates the SOI, which lies between m of 10 and 500. The result of the exploration of this zone is shown in both diagrams in the middle. The next SOI lies between $m = 10$ and $m = 350$ and is explored by m steps of 5. Using this larger resolution, all four transition regions which were expected according to Fig. 10 were found. That means that a minimum m of 350 must be used in order to detect the expected transition regions. Furthermore, a larger value would not effect the significant upward and downward jumps.

spurious subpeaks and random noise. Different lengths of adjacent profiles have almost no effect on the statistical analysis. The method operates on the original profile arrays and focuses on features of profiles that are closely approximate to those of observers only.

Acknowledgments

We thank U. Almert, P. Lau, and E. Mecke of the Institute of Anatomy (University of Lübeck) for their excellent histological preparations, digitizing, and data administration, W. Kühnel and J. Westermann (Institute of Anatomy, Medical University of Lübeck) for their extensive support, S. Prehn (Institute of Technical Informatics, University of Lübeck) for testing, optimizing, and administration the SF 15K computer on which the huge data sets were analyzed. We express our gratitude to A. Wree (Institute of Anatomy, University of Rostock) for his important suggestions and critical discussion of this study. M. Limberg and M. Westlund were of great help editing and correcting the manuscript. This work was supported by the Gerhard Ten Doornkaat Koolman Foundation and the Possehl Foundation.

Appendix

Excess masses

We adapt the original definition of excess mass functionals to the present context: Let $w_1, w_2, \ldots, w_n$ be the gray levels comprising a profile. At first we divide each weight w_i by the overall sum $\Sigma_{j=1}^{n}$ w_j. This leads to probability weights $f_1, f_2, \ldots, f_n$. The mapping

$$\lambda \mapsto \mathbf{E}(\lambda) := \sum_{i=1}^{n} (f_i - \lambda)^+$$

is the *(unrestricted) excess mass functional*, where x^+ stands for $\max(x, 0)$. $\mathbf{E}(\lambda)$ can also be expressed as the maximum of $H(\lambda, C) := \Sigma_{i\in C}(f_i - \lambda)$ over all index sets $C \subset \{1, \ldots, n\}$. An optimal set C is given by $\{i : f_i > \lambda\}$. This set may be divided into maximal index intervals, i.e., sets of consecutive indices. These intervals will be called λ clusters. It is easy to see that the λ clusters concentrate on local maxima of $i \mapsto f_i$ as λ increases. If there are at most M such modes, then for any λ there exist no more than M λ clusters. Next we define the *restricted excess mass functional* as

$$\lambda \mapsto \mathbf{E}_M(\lambda) := \max \sum_{j=1}^{M} H(\lambda, C_j),$$

where the maximum is taken over all collections $C_1, C_2, \ldots, C_M$ of connected index sets C_j such that $C_j \cap C_k = \phi$ for $j \neq k$. Here "connected" means that C_j is either empty or an interval $[a_j, b_j]$ of integers. Note that $f_i > \lambda$ need not hold for all $i \in C_j$, but still $H(\lambda, C_j) \geq 0$. The lemma describes how to obtain $E_{M+1}(\lambda)$ from $E_M(\lambda)$.

Lemma.

Let $C_1^M, \ldots, C_M^M$ be pairwise disjoint connected sets such that $\mathbf{E}_M(\lambda) = \Sigma_{i=1}^{M} H(\lambda, C_i^M)$. Then $\mathbf{E}_{M+1}(\lambda) = \Sigma_{i=1}^{M+1} \times H(\lambda, C_i^{M+1})$, where either

$$\{C_1^{M+1}, \ldots, C_{M+1}^{M+1}\} = \{C_1^M, \ldots, C_M^M\} \cup \{C\}$$

or

$$\{C_1^{M+1}, \ldots, C_{M+1}^{M+1}\} = \{C_1^M, \ldots, C_{i-1}^M, C_{i+1}^M, \ldots, C_M^M\} \cup \{C_I^M \backslash \tilde{C}\}.$$

Here C is a connected set contained in the complement of $C_1^M \cup \ldots \cup C_M^M$ and maximizing $H(\lambda, C)$. Furthermore, I is a number in $\{1, \ldots, M\}$ and $\tilde{C}$ a connected subset of C_I^M such that $H(\lambda, \tilde{C})$ is minimal.

If $H(\lambda, C) > |H(\lambda, \tilde{C})|$, then the new interval C is added. Otherwise C_I^M is split into two intervals by forming the complement $C_I^M \backslash \tilde{C}$.

Figure 12 illustrates the lemma for an arbitrary λ. In the step from $M = 1$ to $M = 2$ the interval that has been found for $M = 1$ is split, since this maximizes the excess mass. The amount of negative mass is greater than the mass that would be contributed by a new interval. In the next step a new interval is added, while finally an old one is split. For $M = 5$ no further changes would occur. Next we give a pseudo code algorithm to compute $E_1(\lambda), \ldots, E_M(\lambda)$ (algorithm 1). Intervals that contribute to the excess mass will be called occupied intervals and the others free intervals. The algorithm uses lists of intervals, where an interval is an object with bounds and a corresponding mass. *LocalMax* is a method that finds an interval with maximal excess mass within a given interval. An efficient implementation, $\mathcal{O}(n)$, of such a procedure is given in Müller and Sawitzki (1991). Note that the intervals always form a partition of $[1, n]$. Hence, the overall complexity of the algorithm is $\mathcal{O}(n \cdot M)$.

For positive integers $M < \tilde{M}$ we define the *excess difference*

$$\Delta_{M,\tilde{M}} := \max_{\lambda} (\mathbf{E}_{\tilde{M}}(\lambda) - \mathbf{E}_M(\lambda)).$$

The maximum is taken over a finite number of λ's that are equidistantly distributed in $[0, \max_i f_i]$. Note that $\Delta_{M,\tilde{M}} = 0$ if $i \mapsto f_i$ has at most M local maxima. Even if it has more than M peaks, but most of them are spurious, then the number $\Delta_{M,\tilde{M}}$ is close to zero. Now we fix such a pair $(M, \tilde{M})$ and compute the excess differences $\Delta_{M,\tilde{M}}$ for all profiles in a given range of the cortex. The basic idea is that if $\Delta_{M,\tilde{M}}$ changes over consecutive profiles, then this is due to a change in the distribution (number or size) of modes.

Algorithm 1 ComputeExcessMass((n, M, $H(\lambda) \rightarrow \{\mathbf{E}_1(\lambda), \ldots, \mathbf{E}_M(\lambda)\}$)
Invariant: The intervals in ListFree and ListOccupied always form a partition of [1, n]
Require: $n \geq M$, all lists are empty
  ListFree.insertInterval([1, n],$H(\lambda, [1, n])$)
  Excess[1. . .M] ← 0
  for $i = 1$ to M do
    ListNewFree.clear
    ListNewOccupied.clear
    /—*find new intervals in free intervals*—/
    for all elements x **in** ListFree **do**
      ListNewFree.insertInterval(x.LocalMax($H(\lambda)$))
    end for
    /—*find intervals with a negative mass in occupied intervals*—/
    for all elements x **in** ListOccupied **do**
      ListNewOccupied.insertInterval(x.LocalMax($-H(\lambda)$))
    end for
    /—*apply lemma 6.1*—/
    if (ListNewFree.getMaxMass>ListNewOccupied.getMaxMass) **then**
      ListFree.splitInterval(ListNewFree.getMaxInterval)
      ListOccupied.insertInterval(ListNewFree.getMaxInterval)
    else
      ListOccupied.splitInterval(ListNewOccupied.getMaxInterval)
      ListFree.insertInterval(ListNewOccupied.getMaxInterval)
    end if
    /—$\mathbf{E}_i(\lambda)$ *is the sum of the masses of all occupied intervals*—/
    Excess[i] ← ListOccupied.getSumMass
  end for
  return(Excess)

Multiple linear rank test

Let Y_i be $\Delta_{M,\tilde{M}}$ for the ith profile. For integers $0 \leq j < k \leq n$ let $R_{j,k}(i)$ be the rank of Y_i among the k–j numbers $Y_{j+1}, \ldots, Y_k$. Then significant changes can be quantified via the local linear rank statistic

$$T_{j,k} := \sum_{i=j+1}^{k} \beta\left(\frac{i-j}{k-j+1}\right) q\left(\frac{R_{j,k}(i)}{k-j+1}\right),$$

with $q(x) := 2x - 1$ and a function β on [0, 1] such that

$$\beta(1-u) = -\beta(u) \text{ for } 0 \leq u \leq 1,$$

$$\beta \geq 0 \text{ on } [0.5, 1].$$

Since we are interested in abrupt changes, in our applications $\beta(x)$ is one of the following:

$$\beta^J(x) = \text{sign}(2x-1) \text{ (Jumps)}$$

$$\beta^{JT}(x) = \text{sign}(2x-1) - (2x-1) \text{ (JumpNTrends)}.$$

The function β^{JT} is less sensitive to gradual changes, which are irrelevant for us, but also slightly less sensitive to real jumps compared with β^J. All local rank statistics are considered simultaneously. For this purpose we define the multiscale test statistic

$$T_m := \max_{0 \leq j < k \leq n : k-j \leq m} (s_{k-j}|T_{j,k}| - c_{k-j})$$

with the norming constants:

$$s_d := d^{-1/2}\sigma(\beta)^{-1}\sigma(q)^{-1}$$

$$c_d := (2\log(n/d))^{1/2},$$

where $\sigma(h)$ denotes the square root of $\int h(x)^2\,dx$. Next we determine a minimal critical value $\kappa(\alpha)$ by means of Monte Carlo simulations such that $P[T_m > \kappa(\alpha)] \leq \alpha$ in case of Y_1, $Y_2, \ldots, Y_n$ being independent and identically distributed random variables. Returning to the original data Y_i, we may claim with confidence $1 - \alpha$ that for *any* pair (j, k) in the sets

$$D^+(\alpha) := \{[j+1,k] : 0 \leq j < k \leq n, s_{k-j}T_{j,k} > c_{k-j} + \kappa(\alpha)\},$$

$$D^-(\alpha) := \{[j+1,k] : 0 \leq j < k \leq n, -s_{k-j}T_{j,k} > c_{k-j} + \kappa(\alpha)\}$$

there is a structural change among the profiles with numbers in $\{j+1, \ldots, k\}$. In order to localize the changes, among all such sets $\{j+1, \ldots, k\}$ we identify the minimal ones. For more detailed information we refer to Dümbgen (2002). Algorithm 2 computes sets $D^+(\alpha)$ and $D^-(\alpha)$ of minimal elements. To guarantee this property, h^- and h^+ ensure that the left endpoints of all pairs taken are pairwise different. In addition the maximal value for the test statistic for every scale d, $2 \leq d \leq m$ is returned (Fig. 2f). In naive implementation the algorithm would need $\mathcal{O}(n^3 \log n)$ steps. With dynamic programming the computation of $\hat{T}$ can be reduced

Algorithm 2 MultipleLocalRankTest (Y, m, $\kappa \to \mathbf{D}^{\pm}(\alpha)$, T_d)

$T_d \leftarrow -c_d$
$\mathbf{D}^{\pm}(\alpha) \leftarrow \phi$
$h^{\pm} \leftarrow 0$
for ($k = 2$ **to** n) **do**
  for ($d = 2$ **to** $\min(k, m)$) **do**
    $\hat{T} \leftarrow \sum_{i=k-d+1}^{k} \beta\left(\frac{i-j}{k-d+1}\right) q\left(\frac{R_{k-d,k(j)}}{d+1}\right)$
    $T_d \leftarrow \max(T_d, s_d|\hat{T}| - c_d)$
    if ($k - d + 1 > h^-$ **and** $-s_d\hat{T} > c_d + \kappa$) **then**
      $\mathbf{D}^-(\alpha) \leftarrow \{\mathbf{D}^-(\alpha), [k - d + 1, k]\}$
      $h^- \leftarrow k - d + 1$
    end if
    if ($k - d + 1 > h^+$ **and** $s_d\hat{T} > c_d + k$) **then**
      $\mathbf{D}^+(\alpha) \leftarrow \{\mathbf{D}^+(\alpha), [k - d + 1, k]\}$
      $h^+ \leftarrow k - d + 1$
    end if
  end for
end for

to constant time in each step of the inner loop. An additional $\mathcal{O}(n)$ space is needed to hold intermediate results from previous steps.

Interval assays

For a given pair (M, $\tilde{M}$), the minimal intervals in $D^+(\alpha)$ and $D^-(\alpha)$ may be visualized as in Fig. 2g. In order to consider many pairs (M, $\tilde{M}$) simultaneously, a more condensed description is needed. For that purpose we compute for each profile index i the numbers

$$B_i^{\pm}(M,\tilde{M}) := \sum_{D\in D^{\pm}(\alpha): i\in D} \text{length}(D)^{-1}.$$

The numbers $B_i^{\pm}$ (M, $\tilde{M}$) are depicted as colored bars in our interval assays. The rows correspond to different pairs (M, $\tilde{M}$), while the profile numbers are listed horizontally. The left and right plots depict the numbers $B^+{}_i$ (M, $\tilde{M}$) and $B^-{}_i$ (M, $\tilde{M}$), respectively.

References

Amunts, K., Klingberg, T., Binkofski, F., Schormann, T., Seitz, R.J., Roland, P., Zilles, K., 1998. Location, asymmetry and variability of human areas 17 and 18. NeuroImage 7, 8.

Amunts, K., Malikovic, A., Mohlberg, H., Schormann, T., Zilles, K., 2000. Brodmann's areas 17 and 18 brought into stereotaxic space—where and how variable? NeuroImage 11, 66–84.

Amunts, K., Schleicher, A., Bürgel, U., Mohlberg, H., Uylings, H., Zilles, K., 1999a. Broca's region revisited: cytoarchitecture and intersubject variability. J. Comp. Neurol. 412, 319–341.

Amunts, K., Schormann, T., Mohlberg, H., Malikovic, A., Zilles, K., 1999b. Location, asymmetry and variability of human areas 17 and 18. NeuroImage 9, 861.

Bailey, P., von Bonin, G., 1951. The Isocortex of Man, Univ. of Illinois Press, Urbana.

Bartels, P., 1979. Numerical evaluation of cytologic data II. Comparison of profiles. Anal. Quant. Cytol. 1, 77–83.

Bartels, P,. 1981. Numerical evaluation of cytologic data VII. Multivariate significance tests. Anal. Quant. Cytol. 3, 1–8.

Blatter, C., 1998. Wavelets–Eine Einführung, Vieweg, Braunschweig.

Braak, H., 1980. Architectonics of the human telencephalic cortex, in: Studies of Brain Function, Springer-Verlag, Berlin.

Brodmann, K., 1909. Vergleichende Lokalisationslehre der Grosshirnrinde in ihren Prinzipien dargestellt auf Grund des Zellenbaues, Barth, Leipzig.

Campbell, A., 1905. Histological Studies on the Localization of Cerebral Function, Cambridge University Press, Cambridge.

Carman, G.J., Drury, H., Essen, D.V., 1995. Computational methods for reconstructing and unfolding the cerebral cortex. Cereb. Cortex 5, 506–517.

Clark, G., 1952. A note on cortical cyto-architectonics. Brain 75, 96–104.

Dümbgen, L., 2002. Application of local rank tests to nonparametric regression. J. Nonparam. Stat. 14, 511–537.

Dunn, O.J., 1961. Multiple comparisons among means. J. Am. Statist. Assoc. 56, 52–64.

Duvernoy, H., 1979. An angioarchitectonic study of the brain. Anat. Clin. 1, 107–222.

Fink, G., Frackowiak, R., Pietrzyk, U., Passingham, R., 1997. Multiple nonprimary motor areas in the human cortex. J. Neurophysiol. 77, 2164–2174.

Fischl, B., Sereno, M., Anders, M., 1999. Cortical surface-based analysis. II: Inflation, flattening, and a surface-based coordinate system. NeuroImage 9, 195–207.

Frackowiak, R., Friston, K., Frith, C., 1997. Human Brain Function, Academic Press, San Diego, CA.

Geyer, S., Ledberg, A., Schleicher, A., Kinomura, S., Schorrmann, T., Buergel, U., Klingberg, T., Larsson, J., Zilles, K., Roland, P., 1996. Two different areas within the primary motor cortex of man. Nature 382, 805–807.

Geyer, S., Matelli, M., Luppino, G., Schleicher, A., Jansen, Y., Palomero-Gallagher, N., Zilles, K., 1998. Receptor autoradiographic mapping of the mesial motor and premotor cortex of the macaque monkey. J. Comp. Neurol. 397, 231–250.

Geyer, S., Schleicher, A., Zilles, K., 1997. The somatosensory cortex of human: cytoarchitecture and regional distributions of receptor-binding sites. NeuroImage 6, 27–45.

Geyer, S., Schleicher, A., Zilles, K., 1999. Areas 3a, 3b, and 1 of human primary somatosensory cortex. 1. Microstructural organization and interindividual variability. NeuroImage 10, 63–83.

Hilbig, H., Bidmon, H., Blohm, U., Zilles, K., 2001. Wisteria floribunda agglutinin labeling patterns in the human cortex: a tool for revealing areal borders and subdivisions in parallel with immunocytochemistry. Anat. Embryol. 203, 45–52.

Hudspeth, A., Ruark, J., Kelly, J., 1976. Cytoarchitectonic mapping by microdensitometry. Proc. Natl. Acad. Sci. USA 73, 2928–2931.

Johansen-Berg, H., Matthews, P., 2002. Attention to movement modulates activity in sensori-motor areas, including primary motor cortex. Exp. Brain Res. 142, 13–24.

Jouandet, M.L., Tramo, M.J., Herron, D.M., Hermann, A., Loftus, W.C., Bazell, J., Gazzaniga, S., 1989. Brainprints: computer-generated two-dimensional maps of the human cerebral cortex in vivo. J. Cogn. Neurosci. 1, 88–117.

Kleist, K., 1934. Gehirnpathologie, Barth, Leipzig.

Krichmar, J., Nasuto, S., 2002. The relationship between neuronal shape and neuronal activity, in: Ascoli, G.A. (Ed.), Computational Neuroanatomy, Humana Press, Totowa, NJ, pp. 105–148.

Lashley, K., Clark, G., 1946. The cytoarchitecture of the cerebral cortex of Ateles: a critical examination of architectonic studies. J. Comp. Neurol. 85, 223–305.

Luppino, G., Matelli, M., Camarda, R., Gallese, V., Rizzolatti, G., 1991. Multiple representations of body movements in mesial area 6 and the adjacent cingulate cortex: an intracortical microstimulation study in the macaque monkey. J. Comp. Neurol. 311, 463–482.

Mahalanobis, P., Majumba, D., Rao, R., 1949. Anthropometric survey of the united provinces. A statistical study. Sankhya Kalkutta 9, 89–101.

Manceaux-Demiau, A., Bryan, R.N., Davatzikos, C., 1998. A probabilistic ribbon model for shape analysis of the cerebral sulci: application to the central sulcus. J. Comput. Assist. Tomography 22, 962–971.

Merker, B., 1983. Silver staining of cell bodies by means of physical development. J. Neurosci. Methods 9, 235–241.

Müller, D., Sawitzki, G., 1991. Excess mass estimates and tests for multimodality. J. Am. Stat. Ass. 86, 738–746.

Naito, E., Ehrsson, H., Geyer, S., Zilles, K., Roland, P., 1999. Illusory arm movements activate cortical motor areas: a positron emission tomography study. J. Neurosci. 19, 6134–6144.

Naito, E., Kinomura, S., Geyer, S., Kawashima, R., Roland, P., Zilles, K., 2000. Fast reaction to different sensory modalities activates common fields in the motor areas, but the anterior cingulate cortex is involved in the speed of reaction. J. Physiol. 83, 1701–1709.

Nieuwenhuys, N., 1985. Chemoarchitecture of the Brain, Springer-Verlag, Berlin.

Orrison, W., Lewine, J., Sanders, J., Hartshorne, M., 1985. Functional Brain Imaging, Mosby, St. Louis.

Peters, T., Williams, J., 1998. The Fourier Transform in Biomedical Engineering, Birkhäuser, Boston.

Pfeifer, R., 1940. Die angioarchitektonische areale Gliederung der Grosshirnrinde, Barth, Leipzig.

Pratt, J., Gibbons, J., 1981. Concepts of Nonparametric Theory, Springer-Verlag, New York.

Preuße, S., Schmitt, O., 1998. Image Analytical Quantification of Immunohistochemical Visualization Techniques Applied to the Human Cerebral Cortex. Borsteler Herbstseminar für Pathologie, Borstel.

Preuße, S., Schmitt, O., 1999a. Quantification and comparison of signal amplification and non-amplificated immunohistochemical reactions of the rat brain by means of image analysis. Elect J. Pathol. Hist. 5.3, 993–10903.

Preuße, S., Schmitt, O., 1999b. Quantitative Immunhistochemie des motorischen und sensorischen Cortex cerebri des Menschen. Ann. Anat. Suppl. 181, 298–299.

Roland, P., Zilles, K., 1996. Functions and structures of the motor cortices in humans. Curr. Opin. Neurobiol. 6, 773–781.

Roland, P., Zilles, K., 1998. Structural divisions and functional fields in the human cerebral cortex. Brain Res. Rev. 26, 87–105.

Sarkissov, S., Filimonoff, I., Kononowa, E., Preobraschenskaja, I., Kukuew, L., 1955. Atlas of the Cytoarchitectonics of the Human Cerebral Cortex, Medgiz, Moscow.

Schleicher, A., Amunts, K., Geyer, S., Kowalski, T., Schormann, T., Palomero-Gallagher, N., Zilles, K., 2000. A stereological approach to human cortical architecture: identification and delineation of cortical areas. J. Chem. Neuroanat. 20, 31–47.

Schleicher, A., Amunts, K., Geyer, S., Kowalski, T., Zilles, K., 1998. Observer-independent cytoarchitectonic mapping of the human cortex using a stereological approach. Acta Stereol. 17, 75–82.

Schleicher, A., Amunts, K., Geyer, S., Morosan, P., Zilles, K., 1999. Observer-independent method for microstructural parcellation of cerebral cortex: a quantitative approach to cytoarchitectonics. NeuroImage 9, 165–177.

Schleicher, A., Ritzdorf, H., Zilles, K., 1986. A quantitative approach to cytoarchitectonics: software and hardware aspects of a system for the evaluation and analysis of structural inhomogeneities in nervous tissue. J. Neurosci. Methods 18, 221–235.

Schleicher, A., Ritzdorf, H., Zilles, K., 1987. Erster Ansatz zur objektiven Lokalisation von Arealgrenzen im Cortex cerebri. Ann. Anat. Suppl. 169, 867–868.

Schleicher, A., Zilles, K., 1990. A quantitative approach to cytoarchitectonics: analysis of structural inhomogeneities in nervous tissue using an image analyser. J. Microsc. 157, 367–381.

Schleicher, A., Zilles, K., Kretschmann, H.-J., 1978. Automatische Registrierung und Auswertung eines Grauwertindex in histologischen Schnitten. Verh. Anat. Ges. 72, 413–415.

Schmitt, O., Böhme, M., 2002. A robust transcortical profile scanner for generating 2D-traverses in histological sections of rich curved cortical courses. NeuroImage 16, 1103–1119.

Schmitt, O., Eggers, R., 1997a. High contrast and homogeneous staining of paraffin sections of whole human brains for three dimensional ultrahigh resolution image analysis. Biotech. Histochem. 73, 44–51.

Schmitt, O., Eggers, R., 1997b. Systematic investigations of the contrast results of histochemical stainings of neurons and glial cells in the human brain by means of image analysis. Micron 28, 197–215.

Schmitt, O., Eggers, R., Haug, H., 2000. Topological distribution of different types of neurons in the human putamen. Anal. Quant. Cytol. Histol. 22, 155–167.

Smith, G., 1907. A new topographical survey of the human cerebral cortex, being an account to the distribution of the anatomically distinct cortical areas and their relationship to the cerebral sulci. J. Anat. 41, 237–254.

Vogt, C., Vogt, O., 1919. Allgemeine Ergebnisse unserer Hirnforschung. J. Psychol. Neurol. 25, 279–461.

von Economo, C., Koskinas, G., 1925. Die Cytoarchitektonik der Hirnrinde des erwachsenen Menschen, Springer-Verlag, Berlin.

Xu, C., Pham, D., Rettmann, M., Yu, D., Prince, J., 1999. Reconstruction of the human cerebral cortex from magnetic resonance images. IEEE T. Med. Imaging 18, 467–480.

Zilles, K., Gross, G., Schleicher, A., Schildgen, S., Bauer, A., Bahro, M., Schwendemann, G., Zech, K., Kolassa, N., 1991. Regional and laminar distributions of α_1-Adrenoceptors and their subtypes in human and rat hippocampus. Neuroscience 40, 307–320.

Zilles, K., Schlaug, G., Geyer, S., Luppino, G., Matelli, M., Schleicher, A., Schormann, T., 1996. Anatomy and transmitter receptors of the supplementary motor areas in the human and nonhuman primate brain. Adv. Neurol. 70, 29–43.

Zilles, K., Schlaug, G., Matelli, M., Luppino, G., Schleicher, A., Qu, M., Dabringhaus, A., Seitz, R., Roland, P., 1995. Mapping of human and macaque sensorimotor areas by integrating architectonic, transmitter receptor, MRI and PET data. J. Anat. 187, 515–537.